UNIVERSITY of York

This is a repository copy of *Kinetic and Desorption Study of Selected Bioactive Compounds on Mesoporous Starbons:A Comparison with Microporous-Activated Carbon*.

White Rose Research Online URL for this paper:
https://eprints.whiterose.ac.uk/id/eprint/142862/

Version: Published Version

Article:
Shannon, James Michael, Clark, James Hanley orcid.org/0000-0002-5860-2480, Ingrid De Heer, Martine et al. (2 more authors) (2018) Kinetic and Desorption Study of Selected Bioactive Compounds on Mesoporous Starbons:A Comparison with Microporous-Activated Carbon. ACS Omega. pp. 18361-18369.

https://doi.org/10.1021/acsomega.8b02602

Reuse
This article is distributed under the terms of the Creative Commons Attribution-NonCommercial-NoDerivs (CC BY-NC-ND) licence. This licence only allows you to download this work and share it with others as long as you credit the authors, but you can't change the article in any way or use it commercially. More information and the full terms of the licence here: https://creativecommons.org/licenses/

Takedown
If you consider content in White Rose Research Online to be in breach of UK law, please notify us by emailing eprints@whiterose.ac.uk including the URL of the record and the reason for the withdrawal request.

White Rose university consortium
Universities of Leeds, Sheffield & York

eprints@whiterose.ac.uk
https://eprints.whiterose.ac.uk/

This is an open access article published under a Creative Commons Non-Commercial No Derivative Works (CC-BY-NC-ND) Attribution License, which permits copying and redistribution of the article, and creation of adaptations, all for non-commercial purposes.

ACS OMEGA

Article

Cite This: ACS Omega 2018, 3, 18361−18369

http://pubs.acs.org/journal/acsodf

Kinetic and Desorption Study of Selected Bioactive Compounds on Mesoporous Starbons: A Comparison with Microporous-Activated Carbon

James Michael Shannon,[†] James Hanley Clark,[†] Martine Ingrid de Heer,[‡] Tobias Ekblad,[§] and Avtar Singh Matharu*[,†]

[†]Green Chemistry Centre of Excellence, University of York, Heslington, YO10 5DD York, U.K.

[‡]Syngenta, Jealotts Hill, Warfield, RG42 6EY Bracknell, U.K.

[§]Maribohilleshög, Säbyholmsvägen 24, 261 91 Landskrona, Sweden

Supporting Information

ABSTRACT: A series of experiments were conducted to determine the chemical and physical differences between varieties of Starbon and activated carbon (AC). The adsorption process for all materials followed pseudo second order kinetics. High levels of adsorption were obtained for all materials; AC showed low levels of desorption for all bioactives over multiple washings, whereas the Starbons showed elevated desorption over the course of multiple washings.

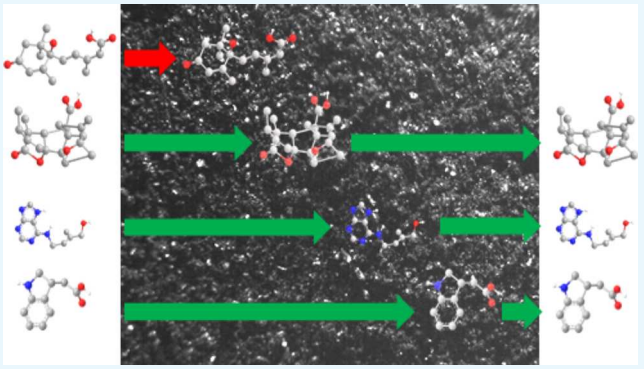

INTRODUCTION

Currently, the UN predicts that world population will increase from 7.3 billion in 2015 to 8.5 billion in 2030.[1] Ensuring a sufficient food supply for an ever-growing and ever-demanding population is of increasing importance while also ensuring that the environment is not adversely affected by intensified agriculture. Thus, to meet the increased demand, methods have been researched to improve crop yields without simultaneously damaging the environment. These include growing crops in new previously inhospitable environments (arid environments), genetically modifying or selectively breeding more robust crop varieties early crop growth and via seed enhancement technologies.[2,3]

Seed enhancement technologies include a range of agro-technical processes performed on the seed prior to planting. Some of these techniques involve applying various materials such as crop protection chemicals, polymers, clays, cellulosic materials (e.g., wood fibres), or activated carbon (AC) to the seed. In a pelleting treatment, the added materials are primarily used to create a consistent size and (near spherical) shape of the seeds, allowing high-precision-mechanized planting, but any such treatment will also have other effects on seed germination and early seedling growth. Seed germination is influenced by both external biotic and abiotic factors along with internal signaling by plant hormones. Hormones can promote (seed growth promoters) or delay (seed growth inhibitors) germination and interact in complex ways with environmental factors.[4−6] Because hormones can also act antagonistically to germination, controlling the buildup and presence of hormones in the direct vicinity of seeds may modulate germination kinetics. This may be achieved by careful selection of the materials used in seed enhancement treatments such as pelleting, ideally allowing the seed to germinate under harsher conditions and thus produce larger yields.[7,8] Hormones are classed by their most pronounced effect on the seed, for example, the gibberellins promote initial plant growth and auxins coordinate plant life cycles, whereas abscisic acid (AA) is produced by the plant to germinate under stressful conditions.[9]

AC is an example of a material used in seed enhancement technology. AC has a high surface area because of its microporous nature (pore size < 2 nm). This high adsorption capacity may be useful for removing plant growth inhibitors from the environment and the seed or for acting as a slow-release matrix for added growth promoters. However, an issue with microporous materials is that some adsorbates may fill or block the pores, reducing the adsorption capacity and preventing desorption of adsorbates inside the micropores. Starbons have a mesoporous structure (pore size of 2−50 nm) which would result in a lower potential adsorption capacity but

Received: September 30, 2018
Accepted: December 12, 2018
Published: December 26, 2018

Downloaded via UNIV OF YORK on February 21, 2019 at 12:06:40 (UTC).
See https://pubs.acs.org/sharingguidelines for options on how to legitimately share published articles.

has little risk of pore blocking while still showing effective adsorption capacity.[10,11] We propose that Starbons would allow plant growth promoters to be slowly released during germination while simultaneously adsorbing plant growth inhibitors from both the environment and the seed, combining both functions into one material to benefit seed germination.

Herein, Starbon materials were tested for their adsorption and desorption behavior of several plant growth promoters and an inhibitor and compared to AC (Figure 1). The chemical

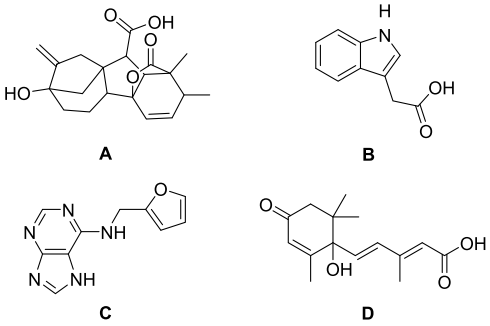

Figure 1. Structures of plant growth promoters [(A) gibberellic acid (GA); (B) indole-3-acetic acid (IAA); and (C) kinetin (KI)] and inhibitor [(D) AA].

and physical properties of Starbon materials depend on the carbonization temperature, in which the precursor material is heated to the desired temperature under vacuum. Lower temperatures (e.g., 100−300 °C) yield a predominantly mesoporous, hydrophilic, and hydroxyl-rich material. At higher temperatures (e.g., 700 °C and above), the structure is still predominantly mesoporous; however, microporosity increases, and the material is less hydrophilic and tending toward zero hydroxyl functionality.[12,13]

A study of molecular volume and diameter (Table 1) showed that GA has a larger molecular volume than the other

Table 1. Physical and Chemical Properties of Plant Growth Promotors and Inhibitor

	density (g/mL)	melting point (°C)	molecular diameter (Nm)	molecular volume ($\times 10^{-22}$ cm^3)	pK_a
GA	0.6	234	1.57	9.58	4.0
IAA	1.2	169	1.21	2.42	4.8
KI	1.5	270	1.48	2.38	2.7
AA	1.2	163	1.50	3.68	4.9

tested plant hormones. This larger size may restrict diffusion through micropores (>2 nm) reducing the overall adsorption capacity. The other plant hormones tested have lower overall volume and would be able to diffuse through the micropores, allowing for a high adsorption capacity compared to GA because of the increased surface area available. The pK_a of each plant hormone was also analyzed, showing that all bar KI had a pK_a of (4−5) and KI was more acidic with a pK_a of 2.7. This would suggest that all of the plant hormones will have a greater interaction with the Starbon surfaces as the temperature of carbonization increases changing the surface functional groups to a more basic and hydrophobic surface.[14]

In this study, we used Starbons prepared at 300, 500, and 800 °C (Starbon A300, Starbon A500, and Starbon A800, respectively) using alginic acid as a precursor with their physical properties listed in Table 2 and compared to AC. The ratio between micro- and mesoporosity is represented as a bar

Table 2. Nitrogen Porosimetry Data for Starbons (A300, A500, and A800) with Respect to AC

	AC	A300	A500	A800
BET surface area/m^2 g^{-1}	525.8	100.1	408.9	459.4
Langmuir surface area/m^2 g^{-1}	730.4	136.0	545.1	610.3
micropore area/m^2 g^{-1}	497.1	63.4	330.1	368.2
micropore volume/cm^3 g^{-1}	0.24	0.03	0.15	0.17
mesopore volume/cm^3 g^{-1}	0.04	0.42	0.46	0.33
percent mesoporosity/%	14	93	75	66

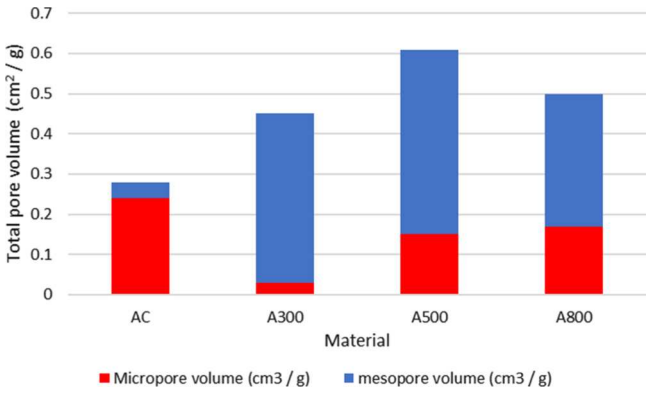

Figure 2. Comparison between micro- and mesopore volume of different materials tested.

chart, as shown in Figure 2. Comparing AC with Starbon 800 shows that Starbon 800 has a Brunauer−Emmett−Teller (BET) surface area comparable to AC while retaining a predominantly mesoporous structure. The mesoporosity for all grades of Starbon reported is higher than that for AC.

On comparison of the isotherms, all Starbons show similar hysteresis loop shapes (Figure 3). AC shows a type H2 loop with very little change between adsorption and desorption with low mesoporosity.[15,16] The H1 hysteresis loop with Starbons confirms that the materials are primarily mesoporous materials.

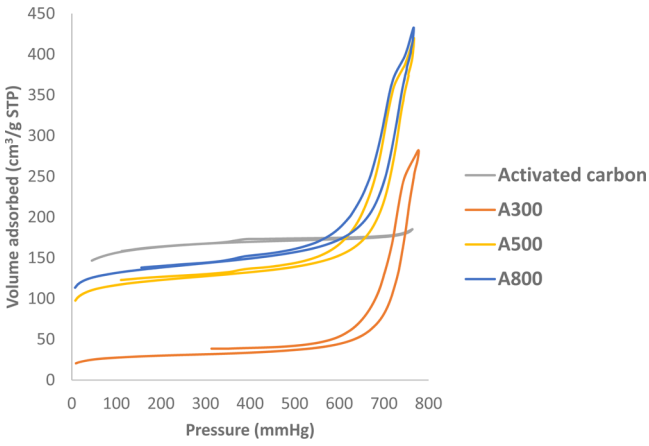

Figure 3. Porosimetry data of mesoporous materials compared to microporous materials.

DOI: 10.1021/acsomega.8b02602
ACS Omega 2018, 3, 18361−18369

At low pressure, AC has the highest recorded adsorption but does not increase significantly after the pressure increases.[17]

When looking at the hysteresis loops, it appears that Starbon materials with their steep decrease during the desorption process follow the type H1 loop suggesting ink-bottle-shaped pores. AC, on the other hand, showed a very small hysteresis loop meaning that there is some mesoporosity, although very little compared to the Starbon material. With its more sloped intermediate but with steep adsorption and desorption points, AC follow a H2 loop with a cylindrical shaped pore and a narrow capillary.

RESULTS AND DISCUSSION

Scanning Electron Microscopy. Starbon samples and AC were analyzed by scanning electron microscopy (SEM). Images were taken at ×750 magnification for all materials (Figure 4).

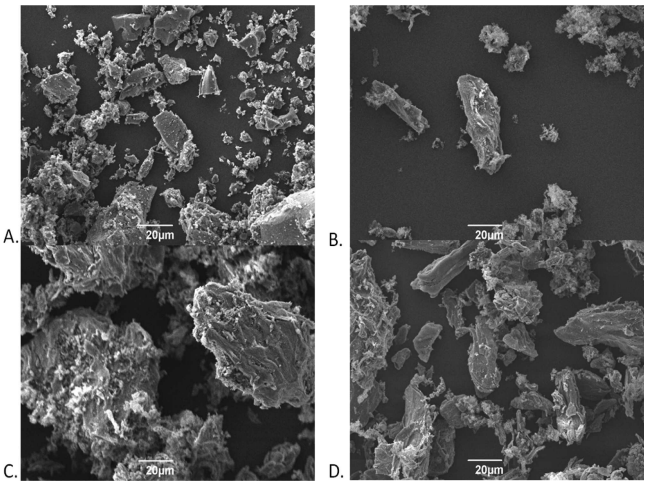

Figure 4. SEM images at ×750 magnification: (A) AC, (B) A300, (C) A500, and (D) A800.

The Starbon samples do not show a smooth surface, particularly for A300 and A500 (Figure 4B,C, respectively). AC (Figure 4A) whilst A800 (Figure 4D) shows smoother surfaces, suggesting that the surface defects observed at lower carbonization temperatures thermally decompose at higher temperatures resulting in less prominent surface defects. AC shows a much greater variety in particle size than may have been expected which may also account for the increased surface area because of the smaller particulate size compared to the Starbon samples. Starbon A500 (Figure 4C) showed particles with a much larger size compared to A800. At higher temperatures, the Starbon material is further carbonized down and decomposes into smaller particulates.[18] The Supporting Information shows the materials analyzed at a higher magnification (Figures S1−S4).

Surface Acidity and Boehm Titration. The surface of the Starbon material has a differing chemistry to the bulk of the material, influencing the adsorption chemistry. Further, the elemental composition and surface chemistry differ depending on the carbonization temperature. This changing surface functionality has a significant effect on the pH at the surface and therefore adsorption interactions.

A pH drift experiment was conducted to determine the point of zero charge (pHpzc; Table 3 and Supporting Information, Figure S5), which is when the pH of a solution in which surface charge of the material has a net neutral charge. If pHpzc is found to be a low pH, then it indicates a more acidic surface, whereas a high pHpzc indicates that the surface has a more basic surface. These results can be compared to both the Boehm titration (Table 4) and the elemental analysis (Table 5) to further understand the surface functionality of the material and how this may affect adsorption.[19−21]

Table 3. pHpzc of Starbons, Precursor, and AC

material	pHpzc
AC	7.9 ± 0.1
A300	6.1 ± 0.2
A500	8.7 ± 0.1
A800	9.2 ± 0.3

Table 4. Boehm Titration Results of Materials Tested

	total acidic groups/mmol				
material	carboxylic groups	lactonic groups	phenolic groups	total	total basic groups/mmol
AC	0.58	0.41	0.70	1.69	2.02
A300	1.44	0.24	0.62	2.39	1.42
A500	0.02	0.19	0.56	0.77	2.75
A800	0.05	0.20	0.51	0.75	3.10

Table 5. Elemental Analysis of Starbon Materials

	C (%)	H (%)	N (%)	other (%)
AA	36.98	4.96		58.06
AC	86.79	0.80	0.16	12.26
A0	31.29	4.80		63.91
A300	63.41	3.85		32.74
A500	75.00	3.01	0.14	21.85
A800	75.19	1.28		23.54

Results show (Table 3 and Figure S5) similarities to previously established work conducted on Starbons with only A800 showing a variation.[15] As expected, Starbon A300 has an acidic surface (pHpzc of 6.1) as it is structurally similar to the Starbon precursor, that is, alginic acid. This acidic nature is due to the oxygen-based functional groups (carbonyls and alcohol groups found on the surface). There is a significant shift in pHpzc between A300 and A500 (6.1−8.7) going from acidic to basic in nature because of the loss of oxygen-based groups and the shift of the remaining functional groups to more anionic structures on the surface as the carbonization temperature increases. A800 shows a higher pHpzc (9.2) than A500 indicating that there has been a continued change to the surface functionality as carbonization increases. This correlates with the information observed in previous work which showed that further carbonization to A800 continues to remove material from the Starbons and further changing the surface chemistry to a graphitic-like nature with strong basicity.[22] AC shows a slightly basic pHpzc of 7.9 which indicates that much of its surface contains more neutral functional groups such as aromatic rings and basic groups.

Boehm titrations were conducted for each Starbon and AC to determine the overall surface functionality (Table 4). A Boehm titration takes the pH drift experiment further to determine what proportion of the surface is acidic and basic. The acidic groups primarily consist of carboxylic acids,

DOI: 10.1021/acsomega.8b02602
ACS Omega 2018, 3, 18361−18369

lactones, and phenolic groups, whereas as the basic group, if detected, then would consist of ketones, pyrones, chromones, and $\pi-\pi$ bonds.[19] Results show that acidic groups were detected on all Starbon materials though in decreasing quantities as the temperature of carbonization increased. This is in line with what was observed in Table 3 which showed that A300 was acidic in nature, whereas both A500 and A800 were basic in nature.

On the basis of the results shown (Table 4), with A300, most of the acidic groups are carboxylic groups and that there are significantly more acidic groups compared to the total number of basic groups, which is in line with the pH drift results. For A500 and A800, there is an observable decrease in the total number of acidic groups mostly because of the decrease in the number of carboxylic groups in A500 and A800. This confirms the results observed via pH drift showing that the surface pH becomes more basic at higher carbonization temperatures, and this is most likely because of decarboxylation which is confirmed via X-ray photoelectron spectroscopy (XPS; see later, Table 5). The results show that A500 and A800 have a similar overall total number of acidic groups but the primary difference between them is the change in total basic groups with A800 having more basic groups on the surface.

Elemental and XPS. Elemental analysis highlights the change in carbon, nitrogen, and oxygen content of the Starbons as the carbonization temperature increases (Table 5). AC shows the highest carbon content and lowest hydrogen content compared to the Starbon materials. Both A300 and A500 showed hydrogen content of over 3% with A800 showing just over 1%. It was noticed that all Starbons tested showed an increasing carbon percentage with the temperature of carbonization because of the thermal degradation removing most of the noncarbonaceous material. Finally, the "other" elements detected are higher for Starbon materials compared to the AC, indicating that Starbons contain several other elements. On the basis of the precursor Starbon (alginic acid), much of this is likely to be oxygen, meaning that Starbons contain a much higher oxygen content than AC.

XPS shows clear trends in the surface functional groups of the Starbon materials (all data may be found in the Supporting Information, Figures S6–S9). It was found that most of the AC surface consisted of C sp^2, which is observed with C=C bonds. Other groups detected were oxygen-based functional groups including carbonyl and carboxylic acids. Finally, $\pi-\pi^*$ bonds were also detected showing aromaticity along with C sp^3 which would mean that the most likely methyl groups would also be on the surface. The remaining functional groups were oxygen based. With A300, $\pi-\pi^*$ bonding was detected at low concentrations. Clearer distinctions for the carbon to oxygen binding energies were reported; hence, it was deduced that carbonyls and carboxylic acid functional groups are on the surface. The presence of C sp^3 groups suggests that methyl groups are on the surface of the material. The XPS for A500 and the results show similarities to A300 but with an increasing proportion of aromatic $\pi-\pi^*$ character and a decreasing amount of oxygen-based functional groups as the oxygen begins to be removed from the material during the carbonization process. These results are expected with the increasing carbonization temperature and agree with elemental analyses. The concentration of C sp^2 peaks increased, showing that there was a greater proportion of C=C and C=O functional groups on the surface. Finally, A800 shows a continuation of the results observed between A300 and A500. There is a decrease in the observed level of oxygen-based functional groups and increase in the carbon-based functional groups, particularly C sp. Of note is that the $\pi-\pi^*$ character has also increased as the temperature of carbonization has increased.

Adsorption Capacity and Kinetic Study. The adsorption of plant hormones on AC and Starbon materials was tested to determine the relationship between adsorption capacity and microporosity (Table 6). During adsorption, the pH was found to fluctuate in acidity (pH 3–5) before the adsorption process to neutral (pH 6.9–7.1) until the adsorption capacity was reached, at which point the pH became more acidic, in line with the increasing concentration of plant hormone tested. It was found that the adsorption capacity increased with microporosity, and therefore the highest overall surface area being able to adsorb the greatest amount of material (Table 2) with AC (730 $m^2\ g^{-1}$) showing the highest adsorption capacity for all adsorbents. Conversely, Starbon 300 (136 $m^2\ g^{-1}$), the most mesoporous material and lowest surface area, had the lowest adsorption capacity, and A800 (610 $m^2\ g^{-1}$) had the highest surface area and adsorption capacity for most plant hormones of the Starbons tested. Of the different plant growth promoters tested, adsorption capacity was the lowest for GA, which was expected because of its bulky structure. The adsorption capacity for KI and IAA was higher than GA for all materials tested. KI was observed to have only a small variance in adsorption capacity with the Starbons and decreased slightly with A800. This would indicate that porosity is not the primary factor that affects the adsorption capacity for KI and is more likely the interaction with the surface. The increased adsorption capacity of IAA and KI compared to GA is most likely because of the small molecular volume (Table 2) compared to GA. IAA and KI also have aromatic structures which also allows for the interaction with the aromatic functional groups on the Starbon because of $\pi-\pi$ stacking.[23−26] The adsorption capacity of the plant growth inhibitor ABA was also found to be greater than GA. This is due to the carboxylic acid group on ABA acting as a primary point of interaction with the adsorbent or other adsorbates, reducing the area required and increasing the number of potentially available adsorption sites. The other potential is the increased adsorbate−adsorbate interaction allowing a multilayer to form, resulting in an increased adsorption capacity.

Table 6. Adsorption Capacity of Materials with Plant Growth Promoters (GA, IAA, and KI) and Inhibitor (ABA)

	adsorption capacity/mg g^{-1}			
hormone	AC	A300	A500	A800
GA	72	98	76	118
IAA	210	115	150	157
KI	205	120	125	121
ABA	314	282	239	370

Kinetic studies were conducted to determine the reaction order of adsorption (Table 7).[27−31] It was observed that in all experiments conducted, none showed a close fit to pseudo first order, for example, (GA on A800, R^2 = 0.003), whereas there was a much closer fit to pseudo second order (GA on A800, R^2 = 0.967).[30] This close fit to pseudo-second-order kinetics suggests that the process of adsorption is a multistep process with multiple physical diffusion steps, with the rate-

DOI: 10.1021/acsomega.8b02602
ACS Omega 2018, 3, 18361−18369

Table 7. Analysis of Materials and Hormones via Pseudo-First-Order Kinetics, Pseudo-Second-Order Kinetics, and the Bangham Isotherm

		R^2/fit to kinetics		
material	hormone	pseudo first	pseudo second	Bangham
AC	GA	0.16 ± 0.01	1.00 ± 0.00	0.94 ± 0.04
	IAA	0.52 ± 0.07	0.99 ± 0.00	0.89 ± 0.09
	KI	0.80 ± 0.09	0.99 ± 0.00	0.97 ± 0.03
	ABA	0.01 ± 0.00	0.99 ± 0.00	0.83 ± 0.08
A300	GA	0.69 ± 0.00	1.00 ± 0.00	0.71 ± 0.07
	IAA	0.20 ± 0.01	0.99 ± 0.00	0.85 ± 0.00
	KI	0.87 ± 0.34	0.99 ± 0.00	0.86 ± 0.06
	ABA	0.23 ± 0.04	0.99 ± 0.13	0.85 ± 0.01
A500	GA	0.35 ± 0.16	0.99 ± 0.00	0.84 ± 0.01
	IAA	0.72 ± 0.00	0.98 ± 0.01	0.81 ± 0.06
	KI	0.92 ± 0.00	0.99 ± 0.00	0.83 ± 0.01
	ABA	0.22 ± 0.01	0.94 ± 0.00	0.87 ± 0.01
A800	GA	0.00 ± 0.00	0.97 ± 0.00	0.99 ± 0.05
	IAA	0.09 ± 0.00	0.99 ± 0.03	0.88 ± 0.02
	KI	0.35 ± 0.01	0.81 ± 0.02	0.92 ± 0.03
	ABA	0.13 ± 0.02	0.93 ± 0.01	0.94 ± 0.06

determining step being attributable to one of these diffusion steps such as mass transport. Most rate-determining steps for adsorption are attributable to mass transport, specifically pore diffusion, and film diffusion or the physico−chemical interaction of the adsorbent and the adsorbate.

The Bangham equation was used to determine the rate-determining step of adsorption.[31] A close fit to the Bangham equation would mean that the rate-determining step has pore diffusion and a high rate of adsorption. The surface area is significant in determining the rate of adsorption with a higher surface area being able to have a higher rate of adsorption because of the increased number of available adsorption sites. This means that AC and A800 as the materials would have the fastest rate of adsorption because of their high surface area (730.4 and 610.3 m^2 g^{-1}, respectively) which is confirmed in the results (Table 7). AC, which has a microporous structure, showed the closest correlation (e.g., GA, R^2 = 0.942) to the Bangham equation (Table 7). For Starbon materials, the data showed a closer fit to the Bangham equation at higher carbonization temperatures (e.g., GA on A800, R^2 = 0.897), which correlates with the increased microporosity of the material, suggesting that pore diffusion is the rate-limiting step for adsorption when the microporosity increases. This also suggests that although pore diffusion impacts the adsorption rate of Starbon 500 and 800, there are additional factors affecting the rate-determining step. Starbon 300 showed the lowest correlation to the Bangham equation suggesting that pore diffusion is not the rate-determining step for this material. Adsorption of the plant growth inhibitor ABA did not follow the Bangham equation for any of the adsorbents tested, suggesting that pore diffusion is not the rate-determining step. On the basis of the experimental data observed, the adsorption process is due to physisorption in which the adsorbates adsorb because of physical interaction with the adsorbent (e.g., hydrogen bonding and van der Waals interactions), rather than through chemisorption which forms a chemical bond during the adsorption process.

Adsorption and Desorption Study. Solid phase extraction (SPE) was used to analyze desorption of hormones from AC and Starbon materials. A low concentration of hormones (10 mg g^{-1}) was adsorbed onto 80 mg of material. Water was selected as the solvent because it is the predominant solvent within agriculture, and calcium chloride was selected to allow controlled impurities into the system because within agriculture, water would not be expected to be deionized.

A summary of the desorption studies is shown in Table 8 with a comparison of materials and bioactives over all washings, as shown in Figure 5. It was observed that the plant growth inhibitor ABA showed poor levels of desorption (less than 1% of the adsorbed material) in all experiments. The Starbons show much greater levels of desorption with the plant growth promoters and a significant improvement over the AC with very low levels of desorption for the plant growth inhibitor. This was an important result as it showed that both AC and the Starbon materials can retain plant growth inhibitors of this type that may prevent or impede seed germination.

Table 8. Total Desorption of Plant Hormones From Materials

	percentage of desorbed material/%			
material	GA	IAA	KI	ABA
AC	0.0 ± 0.0	1.2 ± 0.1	0.0 ± 0.0	0.0 ± 0.0
A300	10.1 ± 2.2	3.7 ± 1.2	26.4 ± 5.6	0.1 ± 0.1
A500	24.8 ± 6.6	14.6 ± 3.2	3.2 ± 0.1	0.5 ± 0.1
A800	19.2 ± 1.8	1.7 ± 1.0	46.8 ± 3.3	0.1 ± 0.1

When testing the plant hormones with AC, it was observed that there was no recorded desorption of GA, KI, or ABA from the AC. Low levels of desorption for IAA from AC was observed (1.2% in total). These results suggest that desorption of the plant hormones from AC is minimal, and thus controlled desorption of plant growth promoters with AC cannot be achieved.

Unlike AC, Starbon 300 showed desorption for all plant growth promoters. GA desorbed 10.0% in total, whereas IAA showed desorption of 3.7%. KI desorbed the largest recorded amount with 26.4%, considerably higher than the other plant growth promoters tested. The plant growth inhibitor, AA, showed low levels of desorption with less than 0.1% desorbed in total. These results indicate that KI has weaker interactions with the adsorbent and so may be more affected by the solvent interactions allowing for higher levels of desorption with the Starbons.

Starbon 500 showed desorption of all plant growth promoters. GA showed the largest desorption at 24.8%. Total desorption was 2.5 times greater than that observed for Starbon 300. This is likely because of the change in the Starbon surface morphology changing from a cellulosic- to an aromatic-like structure during the preparation process, resulting in weaker adsorbate to adsorbent interactions allowing greater desorption.[13,32] IAA desorbed a total of 14.6% which was more than what was observed with AC or Starbon 300. KI desorbed a total of 3.2%; a lower amount than observed with Starbon 300 suggested that KI has become strongly bound at the Starbon surface or was affected by solvent interactions. AA showed low levels of desorption with a total desorption of 0.5%.

Starbon 800 showed high levels of desorption for both GA and KI. GA resulted in a total desorption of 19.2%. IAA recorded a total desorption of 1.7%. They both show a decrease to what was observed with Starbon 500, suggesting

DOI: 10.1021/acsomega.8b02602
ACS Omega 2018, 3, 18361−18369

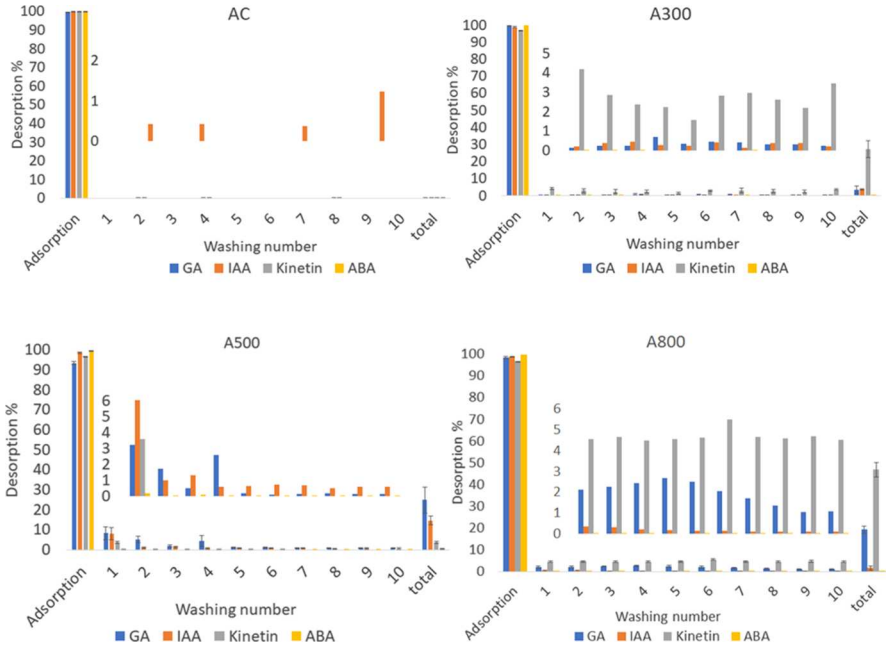

Figure 5. Adsorption and desorption results of bioactives on material (average of four repetitions) (inset shows magnification of desorption washes).

that as the material becomes more hydrophobic, there is greater interaction with the plant growth promoters resulting in a decreased total desorption. KI (KI) showed a high desorption of 31.8%. This suggests that as the material becomes more microporous and hydrophobic in nature, the interactions between KI and the surface have become weaker than that observed with Starbon 500. ABA showed low levels of desorption of 0.1% in total, again showing that Starbons show very low desorption of the plant growth inhibitor.

Figure 5 shows a comparison of desorption of the plant hormones from both AC and Starbon over 10 washings with $CaCl_2/H_2O$. AC showed inconsistent desorption, with only some values leading to a detectable level of desorption. This inconsistent and poor rate of desorption indicate that AC would be very poor as a seed-coating component, designed to promote germination through the release of growth promoters. Starbons, however, showed a more consistent rate of desorption with all plant growth promoters tested. Overall, Starbon results showed that all three plant growth promoters showed consistent, controllable desorption which offers significant possibilities if used as a seed-coating component. In all experiments, the pH of the solvent was measured (6.9−7.0); this could influence the overall desorption interactions, particularly with the Starbons which range from acidic (A300) to basic in nature (A500 and A800). The water solvent can interact more with the Starbon surface (as they dissociate into H^+ and OH^- ions), which may result in increased desorption as the adsorbate interacts.

CONCLUSIONS

Overall, it was concluded that the highly mesoporous nature of Starbons allowed significantly higher levels of desorption with all plant growth promoters than observed with AC. AC, while showing the highest potential adsorption capacity for the selected hormones in most cases, also showed the lowest levels of desorption. It is suspected that this low desorption is due to its microporous nature resulting in pores becoming blocked and preventing desorption from its surface. Starbons, however, dependent on the temperature of carbonizations, particularly A800, show desorption with all selected hormones in all experiments conducted except for ABA which was found to either not desorb or be desorbed at very low quantities (i.e., less than 0.5% in total).

All Starbons tested have shown that they are able to selectively and consistently desorb plant growth promoters while retaining the plant growth inhibitor. This selective retention is potentially useful for seed treatment. Starbons desorbed at different levels depend on the carbonization temperature of the Starbons, this allowed fine tuning of the Starbon performance, something that has the potential to greatly improve current seed enhancement technologies. Future work is underway to further analyze the adsorption isotherms of Starbons using the Langmuir, Freundlich, and Dubinin−Radushkevich equations. Once a model has been developed, germination and field testing can commence at a pilot scale.

EXPERIMENTAL SECTION

Materials and Methodology. Alginic acid derived from brown algae (*Macrocystis pyrifera*, CAS-9005-32-7) was purchased from Bright Moon Seaweed Group (China). AC was supplied by Syngenta, Netherlands, and was produced by Carbotech. Tri-butyl alcohol, KI, IAA, GA, and AA were purchased from Sigma-Aldrich (UK). All writing and analysis was conducted using Microsoft Office unless noted otherwise.

Production of Starbons. Alginic acid (500 g) was placed into a pressure cooker and mixed with water (2 L). The mixture underwent gelation by agitating and heating at 90 °C for 6 h and left to settle for 24 h for the material to undergo retrogradation. The gel then underwent centrifugation using a Thermo Scientific Megafuge 40R centrifuge removing the water from the now solid gel. *tert*-Butyl alcohol (230 g) was mixed into the gel and then freeze-dried to remove the remaining water. The material was then carbonized to the

DOI: 10.1021/acsomega.8b02602
ACS Omega 2018, 3, 18361−18369

required temperature using a Barnstead Thermolyne 600 furnace for 18 h.[15,33−35]

Adsorption Capacity Testing. The adsorbent (50 mg) was placed into a container with deionized water (50 mL) containing increasing quantities of the selected hormone (50, 100, 150, 200, 250, 300, 350, 400, and 500/mg L^{-1}). The solution was analyzed before the addition of the material and agitated for 48 h. The solution was then filtered and analyzed using a Jasco UV−vis spectrometer V-550. Four tests were analyzed to reduce error.[15]

Porosity Testing. Starbon material (100 mg) was deposited into a degassing chamber at 90 °C for 8 h, reweighed, and analyzed via a TriStar porosimeter for 8 h to analyze porosity. Three runs were performed for each material.

pH Drift. Eight batches of the pH solution (50 mL) (pH 3−12) were placed into a glass powder jar. Solutions were made up using a calcium chloride solution (0.1 M) and using hydrochloric acid (0.1 M) and sodium hydroxide (0.1 M) to achieve the required pH. The pH adjustment took place under nitrogen conditions and degassing took place via boiling. A pH probe (Jenway model 6505) was calibrated using buffer solutions and then used to analyze the pH of the solutions. Once analyzed, 50 mg of the expanded material (AC, A00, A300, A500, and A800) was added to each powder jar, sealed, and agitated via a stirrer for 24 h. After 24 h, the stirrer was removed, and the solution settled for 1 h before analyzing via the pH probe. Each experiment was repeated for a total of four times to reduce errors.[36,37]

Boehm Titration. For acidic surfaces, three solutions of 0.05 M NaOH, $NaHCO_3$, and Na_2CO_3 (50 mL) were made up. To each, 1 g of the material was added, purged with nitrogen, and agitated for 12 h. The material was filtered off. Five aliquots of 10 mL solution were taken. Each aliquot was then mixed with 0.05 M solution HCl (20 mL for NaOH and $NaHCO_3$ and 30 mL for Na_2CO_3). The solution was then back-titrated with treated excess NaOH before being back-titrated with the acid solution. For basic surfaces, the same methodology was used but the material was mixed with HCl solution and treated with NaOH solution, treated with excess HCl, and back-titrated with NaOH solution.[38−41]

Titrations were conducted with a 907 Titrando autotitrator and an 804 Titrando stirrer setup. Using a set endpoint pH analysis, the first run would be to pH 5 with an optimum addition rate, following a second titration with the set endpoint of pH 7.1 with a drift of 0.1 pH and a slow set addition of a minimum of 0.10 μL per minute. All five aliquots were analyzed to reduce error.

Elemental Analysis and XPS Analysis. Materials were analyzed by the XPS analysis service provided by the Universality of Cardiff XPS service. A Kratos Axis Ultra DLD system was used to collect the XPS spectra using monochromatic Al Kα X-ray source operating at 120 W (10 mA × 12 kV). Data were collected with pass energies of 160 eV for survey spectra and 40 eV for the high-resolution scans with step sizes of 1 and 0.1 eV, respectively.

The system was operated in the hybrid mode using a combination of magnetic immersion and electrostatic lenses and acquired over an area, approximately 300 × 700 μm^2. A magnetically confined charge-compensation system was used to minimize charging of the sample surface, and all spectra were taken with a 90° take of an angle. A base pressure of ∼1 × 10^{-9} Torr was maintained during the collection of the spectra. Data were analyzed using Casa XPS (v2.3.19rev1.1l) after subtraction of a Shirley background and using modified Wagner sensitivity factors as supplied by the manufacturer.

Adsorption Isotherms and Kinetics. To determine adsorption isotherms, the Starbon material (50 mg) was added to a glass powder jar and filled with calcium chloride solution (0.01 mol/L) (50 mL) (99.8% from Sigma Aldrich) containing different quantities of selected hormone (20, 50, 100, 150, 200, 250, and 300 mg L^{-1}). The solution was agitated via magnetic stirrer for 24 h to achieve equilibrium and analyzed. For a kinetic analysis, the same process was repeated, and readings were taken after 0, 5, 10, 15, 30, 60, and 240 min. Samples of the solution were analyzed via a Jasco UV−vis spectrometer V-550 (see the Supporting Information for calibration plot of standards and an exemplar UV−vis plot for kinetic, Figures S10 and S11, respectively). This was repeated four times for each material to reduce error. The model of the linearized pseudo-first-order plot was used (eq 1)[42,43]

$$\log(q_e - q_t) = -\frac{k_1}{2.303}t + \log(q_e) \quad (1)$$

In which, q_e = amount of material adsorbed at equilibrium (mg g^{-1}), q_t = amount of material adsorbed at time (mg g^{-1}), t = time (min), and k_1 = pseudo-first-order rate constant (min^{-1}). For modeling of the pseudo second order, the following linear equation was used (eq 2)

$$\frac{t}{q_t} = \frac{1}{k_2 q_e^{\,2}} + \frac{1}{q_e}t \quad (2)$$

where k_2 represents the pseudo-second-order rate constant. Finally, the Bangham model (eq 3) was used

$$\log\left(\frac{q_e}{q_e - q_t m}\right) = \log\left(\frac{kbm}{2.303V}\right) + a \log t \quad (3)$$

with a and kb both being constants, v = volume of the solution (L), and m = mass of the adsorbate (g/L).

Adsorption and Desorption Testing of Plant Hormones. To test adsorption and desorption, the Starbon material (80 mg) was placed into an SPE cartridge and sealed. Deionized water (10 mL) was drained through the expanded material to condition the cartridge and then rewashed using deionized water (10 mL). Plant hormone solution (375 μL) was mixed with calcium chloride solution (0.01 mol/L) (50 mL) (99.8% from Sigma-Aldrich) and was used as the solvent to simulate impurities in natural water and drained through the SPE cartridge (0.5 mL min^{-1}). The cartridge was then left to dry under vacuum for 30 min; all experiments were conducted at room temperature (18 °C). Finally, to collect the data of desorption, deionized water (5 mL) was drained through the SPE cartridge (0.5 mL min^{-1}) and collected for analysis, this process was repeated for a total of 10 times (50 mL). Each experiment was repeated for a total of four experiments. Analysis was conducted using a Shimadzu Prominence HPLC with an Athena C18-WP 250 × 4.6 mm, 5 μm column. Initial equilibration was conducted using deionized water (0.1% formic acid)/acetonitrile at a 90:10 mix and was run for 5 min and repeated a minimum of three times. The primary run was a deionized water (0.1% formic acid)/acetonitrile at a 90:10 mix shifting to 10:90 over the course of a 30 min run.[44−46]

DOI: 10.1021/acsomega.8b02602
ACS Omega 2018, 3, 18361−18369

■ ASSOCIATED CONTENT

Supporting Information

The Supporting Information is available free of charge on the ACS Publications website at DOI: 10.1021/acsomega.8b02602.

SEM image of AC and A300 at ×6000 magnification, A500 at ×2500 magnification, A800 at ×2000 and ×15,000 magnification; pH drift and determination of pHpzc; XPS analysis of AC, A300, A500, and A800; calibration graph for UV-vis analysis; and exemplar of UV-vis (PDF)

■ AUTHOR INFORMATION

Corresponding Author

*E-mail: avtar.matharu@york.ac.uk (A.S.M.).

ORCID

James Hanley Clark: 0000-0002-5860-2480

Avtar Singh Matharu: 0000-0002-9488-565X

Notes

The authors declare no competing financial interest.

■ ACKNOWLEDGMENTS

A.S.M. would like to acknowledge Syngenta for sponsoring J.M.S. for the PhD study and provision of AC.

■ REFERENCES

(1) Gerland, P.; Raftery, A. E.; Sevčíková, H.; Li, N.; Gu, D.; Spoorenberg, T.; Alkema, L.; Fosdick, B. K.; Chunn, J.; Lalic, N.; et al. World Population Stabilization Unlikely This Century. *Science* **2014**, *346*, 234−237.

(2) Huang, K.; Chai, S.-H.; Mayes, R. T.; Tan, S.; Jones, C. W.; Dai, S. Significantly Increasing Porosity of Mesoporous Carbon by $NaNH_2$ Activation for Enhanced CO2 Adsorption. *Microporous Mesoporous Mater.* **2016**, *230*, 100−108.

(3) Khan, M. N.; Mobin, M.; Abbas, Z. K.; AlMutairi, K. A.; Siddiqui, Z. H. Role of Nanomaterials in Plants under Challenging Environments. *Plant Physiol. Biochem.* **2016**, *110*, 194−209.

(4) Huang, Y.; Cai, S.; Ye, L.; Hu, H.; Li, C.; Zhang, G. The Effects of GA and ABA Treatments on Metabolite Profile of Germinating Barley. *Food Chem.* **2016**, *192*, 928−933.

(5) Suman, M.; Meghawal, D. R.; Sahu, O. P.; Mahaveer, C.; Senior, S.; Fellow, R.; Sangma, P. D. Effect of Plant Growth Regulators on Fruit Crops. *J. Pharmacogn. Phytochem.* **2017**, *331*, 331−337.

(6) Richards, D. E.; King, K. E.; Ait-Ali, T.; Harberd, N. P. How Gibberellin Regulates Plant Growth and Development: A Molecular Genetic Analysis Of Gibberellin Signaling. *Annu. Rev. Plant Physiol. Plant Mol. Biol.* **2001**, *52*, 67−88.

(7) Bala Raju, B.; Prashant, K. R. Studies on Effect of Polymer Seed Coating, Nanoparticles and Hydro Priming on Seedling Characters of Pigeonpea (Cajanus Cajan L.) Seed. *J. Pharmacogn. Phytochem.* **2017**, *6* (4), 140−145.

(8) Madsen, M. D.; Davies, K. W.; Boyd, C. S.; Kerby, J. D.; Svejcar, T. J. Emerging Seed Enhancement Technologies for Overcoming Barriers to Restoration. *Restor. Ecol.* **2016**, *24*, 77−84.

(9) Yang, Z. Small GTPases: Versatile Signaling Switches in Plants. *Plant Cell* **2002**, *14*, 375−388.

(10) Galán, J.; Rodríguez, A.; Gómez, J. M.; Allen, S. J.; Walker, G. M. Reactive Dye Adsorption onto a Novel Mesoporous Carbon. *Chem. Eng. J.* **2013**, *219*, 62−68.

(11) Tanthapanichakoon, W.; Ariyadejwanich, P.; Japthong, P.; Nakagawa, K.; Mukai, S. R.; Tamon, H. Adsorption−desorption Characteristics of Phenol and Reactive Dyes from Aqueous Solution on Mesoporous Activated Carbon Prepared from Waste Tires. *Water Res.* **2005**, *39*, 1347−1353.

(12) Figueiredo, J. L. Functionalization of Porous Carbons for Catalytic Applications. *J. Mater. Chem. A* **2013**, *1*, 9351.

(13) Shuttleworth, P. S.; Budarin, V.; White, R. J.; Gun'ko, V. M.; Luque, R.; Clark, J. H. Molecular-Level Understanding of the Carbonisation of Polysaccharides. *Chemistry* **2013**, *19*, 9351−9357.

(14) Budarin, V.; Clark, J. H.; Hardy, J. J. E.; Luque, R.; Milkowski, K.; Tavener, S. J.; Wilson, A. J. Starbons: New Starch-Derived Mesoporous Carbonaceous Materials with Tunable Properties. *Angew. Chem., Int. Ed.* **2006**, *118*, 3866−3870.

(15) Borisova, A. Advances in Characterisation , Preparation and Application of Polysaccharide-Derived Mesoporous Carbons for Environmental Remediation. PhD Thesis, University of York, 2015.

(16) White, R. J.; Budarin, V.; Luque, R.; Clark, J. H.; Macquarrie, D. J. Tuneable Porous Carbonaceous Materials from Renewable Resources. *Chem. Soc. Rev.* **2009**, *38*, 3401.

(17) Ku, K. H.; Shin, J. M.; Klinger, D.; Jang, S. G.; Hayward, R. C.; Hawker, C. J.; Kim, B. J. Particles with Tunable Porosity and Morphology by Controlling Interfacial Instability in Block Copolymer Emulsions. *ACS Nano* **2016**, *10*, 5243−5251.

(18) Goldstein, J.; Newbury, D. E.; Michael, J. R.; Ritchie, N. W. M.; Scott, J. H. J.; Joy, D. C. *Scanning Electron Microscopy and X-Ray Microanalysis*, 4th ed.; Springer, 2018.

(19) Rivera-Utrilla, J.; Bautista-Toledo, I.; Ferro-García, M. A.; Moreno-Castilla, C. Activated carbon surface modifications by adsorption of bacteria and their effect on aqueous lead adsorption. *J. Chem. Technol. Biotechnol.* **2001**, *1*, 1209−1215.

(20) Gomes, H. T.; Miranda, S. M.; Sampaio, M. J.; Sampaio, A. M. T.; Faria, J. L. Activated Carbons Treated with Sulphuric Acid: Catalysts for Catalytic Wet Peroxide Oxidation. *Catal. Today* **2010**, *151*, 153−158.

(21) Al-Degs, Y. S.; El-Barghouthi, M.; et al. Effect of Solution PH, Ionic Strength, and Temperature on Adsorption Behavior of Reactive Dyes on Activated Carbon. *Dyes Pigm.* **2008**, *77*, 16−23.

(22) Muñoz García, A.; Hunt, A. J.; Budarin, V. L.; Parker, H. L.; Shuttleworth, P. S.; Ellis, G. J.; Clark, J. H. Starch-Derived Carbonaceous Mesoporous Materials (Starbon) for the Selective Adsorption and Recovery of Critical Metals. *Green Chem.* **2015**, *17*, 2146−2149.

(23) Libbrecht, W.; Verberckmoes, A.; Thybaut, J. W.; Van Der Voort, P.; De Clercq, J. Tunable Large Pore Mesoporous Carbons for the Enhanced Adsorption of Humic Acid. *Langmuir* **2017**, *33*, 6769−6777.

(24) Björk, J.; Hanke, F.; Palma, C.-A.; Samori, P.; Cecchini, M.; Persson, M. Adsorption of Aromatic and Anti-Aromatic Systems on Graphene through Π−π Stacking. *J. Phys. Chem. Lett.* **2010**, *1*, 3407−3412.

(25) Shi, Y.; van Steenbergen, M. J.; Teunissen, E. A.; Novo, L.; Gradmann, S.; Baldus, M.; van Nostrum, C. F.; Hennink, W. E. Π−Π Stacking Increases the Stability and Loading Capacity of Thermosensitive Polymeric Micelles for Chemotherapeutic Drugs. *Biomacromolecules* **2013**, *14*, 1826−1837.

(26) Bulut, Y.; Aydın, H. A Kinetics and Thermodynamics Study of Methylene Blue Adsorption on Wheat Shells. *Desalination* **2006**, *194*, 259−267.

(27) Ho, Y. S.; McKay, G. Pseudo-Second Order Model for Sorption Processes. *Process Biochem.* **1999**, *34*, 451−465.

(28) Chakrapani, C.; Babu, C.; Vani, K.; Somasekhara Rao, K. Adsorption Kinetics for the Removal of Fluoride from Aqueous Solution by Activated Carbon Adsorbents Derived from the Peels of Selected Citrus Fruits. *E J. Chem.* **2010**, *7*, 419−427.

(29) Srivastava, V. C.; Swamy, M. M.; Mall, I. D.; Prasad, B.; Mishra, I. M. Adsorptive Removal of Phenol by Bagasse Fly Ash and Activated Carbon: Equilibrium, Kinetics and Thermodynamics. *Colloids Surf., A* **2006**, *272*, 89−104.

(30) Simonin, J.-P. On the Comparison of Pseudo-First Order and Pseudo-Second Order Rate Laws in the Modeling of Adsorption Kinetics. *Chem. Eng. J.* **2016**, *300*, 254−263.

(31) Yakout, S. M.; Elsherif, E. Batch Kinetics, Isotherm and Thermodynamic Studies of Adsorption of Strontium from Aqueous

DOI: 10.1021/acsomega.8b02602
ACS Omega 2018, 3, 18361−18369

Solutions onto Low Cost Rice-Straw Based Carbons. *Carbon: Sci. Technol.* **2010**, *1*, 144−153.
(32) Marriott, A. S.; Hunt, A. J.; Bergström, E.; Thomas-Oates, J.; Clark, J. H. Effect of Rate of Pyrolysis on the Textural Properties of Naturally-Templated Porous Carbons from Alginic Acid. *J. Anal. Appl. Pyrolysis* **2016**, *121*, 62−66.
(33) Parker, H. L. Recovery from Waste Streams: Working Towards a Sustainable Future. PhD thesis, University of York, 2013.
(34) STARBONS: Preparation, applications and transition from laboratory curiosity to scalable product. http://www.nsti.org/procs/Nanotech2011v3/11/W5.162 (accessed May 17, 2016).
(35) Parker, H. L.; Budarin, V. L.; Clark, J. H.; Hunt, A. J. Use of Starbon for the Adsorption and Desorption of Phenols. *ACS Sustainable Chem. Eng.* **2013**, *1*, 1311−1318.
(36) Al-Degs, Y. S.; El-Barghouthi, M. I.; El-Sheikh, A. H.; Walker, G. M. Effect of Solution PH, Ionic Strength, and Temperature on Adsorption Behavior of Reactive Dyes on Activated Carbon. *Dyes Pigm.* **2008**, *77*, 16−23.
(37) Rivera-Utrilla, J.; Bautista-Toledo, I.; Ferro-García, M. A.; Moreno-Castilla, C. Activated Carbon Surface Modifications by Adsorption of Bacteria and Their Effect on Aqueous Lead Adsorption. *J. Chem. Technol. Biotechnol.* **2001**, *76*, 1209−1215.
(38) Leon y Leon, C. A.; Solar, J. M.; Calemma, V.; Radovic, L. R. Evidence for the Protonation of Basal Plane Sites on Carbon. *Carbon* **1992**, *30*, 797−811.
(39) Goertzen, S. L.; Thériault, K. D.; Oickle, A. M.; Tarasuk, A. C.; Andreas, H. A. Standardization of the Boehm Titration. Part I. CO2 Expulsion and Endpoint Determination. *Carbon* **2010**, *48*, 1252−1261.
(40) Oickle, A. M.; Goertzen, S. L.; Hopper, K. R.; Abdalla, Y. O.; Andreas, H. A. Standardization of the Boehm Titration: Part II. Method of Agitation, Effect of Filtering and Dilute Titrant. *Carbon* **2010**, *48*, 3313−3322.
(41) Contescu, A.; Contescu, C.; Putyera, K.; Schwarz, J. A. Surface Acidity of Carbons Characterized by Their Continuous PK Distribution and Boehm Titration. *Carbon* **1997**, *35*, 83−94.
(42) Limousin, G.; Gaudet, J.-P.; Charlet, L.; Szenknect, S.; Barthès, V.; Krimissa, M. Sorption Isotherms: A Review on Physical Bases, Modeling and Measurement. *Appl. Geochem.* **2007**, *22*, 249−275.
(43) Ho, Y.-S. Review of Second-Order Models for Adsorption Systems. *J. Hazard. Mater.* **2006**, *136*, 681−689.
(44) Ravelo-Pérez, L. M.; Hernández-Borges, J.; Rodríguez-Delgado, M. Á. Multi-Walled Carbon Nanotubes as Efficient Solid-Phase Extraction Materials of Organophosphorus Pesticides from Apple, Grape, Orange and Pineapple Fruit Juices. *J. Chromatogr. A* **2008**, *1211*, 33−42.
(45) Ivanov Dobrev, P.; Kamínek, M. Fast and Efficient Separation of Cytokinins from Auxin and Abscisic Acid and Their Purification Using Mixed-Mode Solid-Phase Extraction. *J. Chromatogr. A* **2002**, *950*, 21−29.
(46) Płotka-Wasylka, J.; Szczepańska, N.; de la Guardia, M.; Namieśnik, J. Modern Trends in Solid Phase Extraction: New Sorbent Media. *TrAC, Trends Anal. Chem.* **2016**, *77*, 23−43.

DOI: 10.1021/acsomega.8b02602
ACS Omega 2018, 3, 18361−18369